JJMIE

Volume 11 Number 4, December. 2017
ISSN 1995-6665
Pages 201 -207

Jordan Journal of Mechanical and Industrial Engineering

Co-Firing of Petroleum Coke Waste and Kentucky Coal in an Entrained Flow Gasifier

Isam Janajreh [a *], Idowu Adeyemi [a], Chaouki Ghenai [b]

[a] *Mechanical and Materials Engineering Department, Khalifa University of Science and Technology, Masdar Institute, P. O. Box 54224, Abu Dhabi, UAE,*

[b] *Sustainable and Renewable Energy Engineering Department, University of Sharjah, P. O. Box 27272, Sharjah UAE*

Abstract

In the present study, a numerical model for the gasification of a mixture of Kentucky Coal and Petroleum Coke inside an oxygen-fed atmospheric Entrained Flow Gasifier (EFG) is developed. Three mixing percentages of petroleum coke (10%, 25% and 50%) are studied. The Kentucky coal was characterized with Thermo-Gravimetric Analyzer (TGA) for the proximate analysis, Flash 2000 for the ultimate analysis and bomb calorimeter (Parr 6100). The model is based on the Lagrangian-Eulerian approach whereby the solid phase particles are tracked with the Lagrangian approach and the surrounding gas phase is tracked by the Eulerian phase. The model takes into account the turbulent flow for the continuous phase (Realizable k-ε model), gas phase gasification (Species transport model), devolatalization (Kobayashi two competing rate model), heterogeneous char reaction (Multiple surface reaction model), particle dispersion by turbulent flow (Stochastic discrete random walk model), radiation (P1) and particle distribution (Rosin rammler model). The effect of petcock percentage, wall temperature and the particle size on gas composition and gasification metric has been studied. The present study shows that decreasing the particle size does not lead to the production of more SynGas (CO+H2). Particle size of 334nm led to the highest SynGas production and lowest exit temperature. Marinating a wall temperature at 1,173 K led to the production of the most SynGas.

1. Introduction

Petroleum coke (petcoke) is the byproduct of the refining process. It is characterized with a high heating value and low ash contents. However, it is often difficult to utilize as a stand-alone feedstock because of its low volatile fraction which makes it challenging to ignite additional to its high sulfur contents. It is therefore often blended with coal to compensate the lack of volatility by improve its ignition and reduce its emission. Moreover, petcoke cost offers significant advantages for coal plants as it is quite inexpensive. Although there are various numerical 2-D and 3-D models for the entrained flow gasification of coal particles in the literature [1-4], there is no study which has focused on the numerical modelling of the entrained flow gasification of the mixture of Kentucky coal and Petroleum coke. For example, Hampp [1] developed a 2D model for the gasification of Kentucky coal inside a drop tube reactor (DTR). Chen et al. [2] developed a 3-D simulation model for an air-blown 200 ton/day two-stage entrained flow gasifier, they used numerical methods and sub-models conventionally for pulverized coal combustion. Watanabe *et al.* [3] performed multi-dimensional computational modeling of an entrained flow gasifier for coal gasification with the Langrangian-Eulerian based approach. Abani and Ghoniem [4] developed a model for a 3-D multiphase reacting flow in a coal fed entrained flow gasifier using Large Eddy Simulation (LES) –with a one-equation eddy viscosity model- and Reynolds-Averaged Navier Stokes (RANS) – that account for gas phase turbulence. Ghenai and Janajreh [5] studied the effect of biomass (wheat straw) addition to bituminous coal on the reactor centerline NO_x and CO_2 concentration. They discovered that the NO_x and CO_2 concentration decreased along the centerline with the addition of wheat straw. The gasification of Kentucky coal and higher volatile woody biomass have been recently carried out by authors under different gasification parameters, i.e., equivalence ratio, pressure and temperature [6]. Additional to the high fidelity simulation, an experimental work was conducted in the air-blown atmospheric DTR experimental facility at the Waste-2-Energy Laboratory at Masdar Institute. The measured centerline temperature, exit gas composition, and SEM images were obtained and used for the model validation and more understanding has been gained in the gasification of these two different feedstock particles. In another work by the present authors, macro algae was used and co-gasified with coal by avoiding the many processes of its lipid extraction and conversion [7]. The gasification done under CO_2 and H_2O moderation following both

* Corresponding author e-mail: ijanajreh@masdar.ac.ae.

equilibrium and high fidelity. The H_2O lead to higher gasification efficiency of nearly eight points compared to CO_2.

Nevertheless, there has been no known study of the numerical modeling of the entrained flow gasification of the mixture of petcoke and coal in the literature. The objective of the present study is to develop a numerical model for the entrained flow gasification of the mixture of petroleum coke and Kentucky coal using the Lagrangian-Eulerian approach. The present work also attempts to optimize the developed model following parametric study of the effect of the petcoke mixture percentage, gasifier's wall temperature and particle size on the gasification of the mixture.

2. Material Characterization

The material characterization of the Kentucky coal was conducted at the Masdar Institute Waste to Energy Laboratory. The Thermo-Gravimetric Analyzer (TGA) and Flash CHNOS-elemental analyzer are used to determine the proximate and ultimate analyses of the Kentucky coal. These were used the basis to determine the characteristics of the Kentucky-coal-petroleum coke mixture. The data for the characterization of the petroleum coke were obtained from the literature [8]. The characterization gives an insight into the composition of feedstock before further analysis. The elemental analysis is necessary to infer the chemical formula of the feedstock, or unit molecular weight, to regulate the stoichiometry of the oxidizer/moderator gases and estimate enthalpy of reaction [9-12]. The proximate analysis help in the proper selection of devolatilization, moisture release and char combustion models. The proximate and ultimate analysis data for the Kentucky coal-petcoke mixture at 10%, 25% and 50% of petcoke are as depicted in Tables 1-2. For the ultimate analysis, samples of the Kentucky coal in tin capsules were placed into an oxidation-reduction reactor of temperature between 900 and 1000 ^oC. This causes the samples to combust, generating large amount of heat while raising the temperature in the reactor to around 1,800 ^oC. At this high temperature, all organic and inorganic fractions are converted into elements. These elemental composition are carried to the chromatography column and identified quantitatively via the Thermal Conductivity Detectors (TCD).

Table 1: Ultimate analyses of coal and petroleum coke

Ultimate (mass %)	Petroleum Coke (10%)	Petroleum Coke (25%)	Petroleum Coke (50%)
C	77.879	79.9775	83.475
H	5.187	5.1075	4.975
N	2.183	1.9775	1.635
O	7.573	6.5275	4.785
S	1.183	1.3675	1.675
A	5.995	5.0425	3.455
Total	100	100	100

Table 2: Proximate analyses and heating value of coal and petroleum coke

Proximate (mass %)	Petroleum Coke (10%)	Petroleum Coke (25%)	Petroleum Coke (50%)
M	2.411	2.0225	1.375
V	37.106	33.395	27.21
FC	54.488	59.54	67.96
A	5.995	5.0425	3.455
Total	100	100	100
LHV (MJ/kg)	30.848	31.49	32.56

3. Model Development

The gasification of the feedstock includes several processes including moisture release, devolatilization, gas phase reactions and char combustion. These processes can be summarized as shown below:

$$Feedstock_s \rightarrow Volatile_s + Char_s + Steam \quad (1)$$

$$Volatile_s \rightarrow \alpha_1 CH_4 + \alpha_2 CO + \alpha_3 CO_2 + \alpha_4 H_2 + \alpha_5 H_2O + \alpha_6 Tar \quad (2)$$

$$C_s Ash + 0.5O_2 \rightarrow CO + Ash \quad (3)$$

$$C_s Ash + CO_2 \rightarrow 2CO + Ash \quad (4)$$

$$C_s Ash + H_2O \rightarrow CO + H_2 + Ash \quad (5)$$

As soon as the feedstock is injected into the gasifier, the moisture is dried out then volatiles is released according to equations 1 and 2. At this stage, several homogenous/volumic reactions take place which follow their own reaction kinetics. Common homogenous coal reactions and their associated kinetics are summarized in Table 3 [13].

Table 3: Kinetic Data for the Homogeneous Reactions

Reaction	Activation Energy (E_a)	Pre-Exponential Factor (A)	Reaction Order (N)
$CH_4 + \frac{1}{2}O_2 \rightarrow CO + 2H_2$	1.25×10^8	4.4×10^{11}	0
$H_2 + \frac{1}{2}O_2 \rightarrow H_2O$	1.67×10^8	6.8×10^{15}	-1
$CO + \frac{1}{2}O_2 \rightarrow CO_2$	1.67×10^8	2.24×10^{12}	0
$CH_4 + H_2O \rightarrow CO + 3H_2$	1.25×10^8	3×10^8	0
$CO + H_2O \rightarrow CO_2 + H_2$	8.37×10^7	2.75×10^9	0

The remaining char then undergoes into a series of heterogeneous/surface gasification reactions (Equations 3-5), namely exothermic char-O_2, the two endothermic char-CO_2 and char-H_2O. They follow 1st order Arrhenius rate as listed in Table 4 [14, 15].

Table 4: Kinetic Data for the Arrhenius heterogeneous reactions

Reaction	Activation Energy, E_a (J/mol)	Pre-Exponential Factor (A)	Reaction Order (n)
$C + \frac{1}{2}O_2 \rightarrow CO$	9.23×10^7	2.3	1
$C + CO_2 \rightarrow 2CO$	1.62×10^8	4.4	1
$C + H_2O \rightarrow CO + H_2$	1.47×10^8	1.33	1

3.1. Modeling Equations

In order to correctly model this phenomenon, mass, momentum, energy and species have to be conserved following the conservation of mass transport equation 6 below:

$$\frac{\partial \rho}{\partial t} + \frac{\partial(\rho v_x)}{\partial t} + \frac{\partial(\rho v_r)}{\partial t} + \frac{\rho v_r}{r} = S_m \quad (6)$$

where ρ is the density and upper case S_m is the source terms due to the dispersed/discrete phase interaction. The transport of density-velocity multiple (ρ u_x) and the density-energy multiple (ρE) represent the conservation of momentum and energy, respectively, and these are written in Eqs. 7 and 10 as:

$$\frac{\partial(\rho v_x)}{\partial t} + \frac{1}{r}\frac{\partial}{\partial x}(r\rho v_x v_x) + \frac{1}{r}\frac{\partial}{\partial r}(r\rho v_r v_x) = -\frac{\partial p}{\partial x} + \frac{1}{r}\frac{\partial}{\partial x}\left[\mathrm{r}\mu\left(2\frac{\partial v_x}{\partial x} - \frac{2}{3}(\nabla\cdot\vec{v})\right)\right] + \frac{1}{r}\frac{\partial}{\partial r}\left[\mathrm{r}\mu\left(\frac{\partial v_x}{\partial r} + \frac{\partial v_r}{\partial x}\right)\right] + F_x \quad (7)$$

$$\frac{\partial(\rho v_r)}{\partial t} + \frac{1}{r}\frac{\partial}{\partial x}(r\rho v_x v_r) + \frac{1}{r}\frac{\partial}{\partial r}(r\rho v_r v_r) = -\frac{\partial p}{\partial x} + \frac{1}{r}\frac{\partial}{\partial x}\left[\mathrm{r}\mu\left(\frac{\partial v_x}{\partial r} + \frac{\partial v_r}{\partial x}\right)\right] + \frac{1}{r}\frac{\partial}{\partial r}\left[\mathrm{r}\mu\left(2\frac{\partial v_r}{\partial r} - \frac{2}{3}(\nabla\cdot\vec{v})\right)\right] - 2\mu\frac{v_r}{r^2} + \frac{2}{3}\frac{\mu}{r}(\nabla\cdot\vec{v}) + \rho\frac{{v_z}^2}{r} + F_r \quad (8)$$

where p is the pressure, μ is the fluid viscosity, and F_x is the present body forces in the form of gravitational force and the divergence of the velocity is expressed as:

$$(\nabla\cdot\vec{v}) = \frac{\partial v_x}{\partial x} + \frac{\partial v_r}{\partial r} + \frac{v_r}{r} \quad (9)$$

$$\frac{\partial(\rho E)}{\partial t} + \nabla\cdot\left(\vec{v}(\rho E + p)\right) = \nabla\cdot\left(k_{eff}\nabla T - \sum_j h_j\vec{J}_j + (\bar{\bar{\tau}}_{eff}\cdot\vec{v})\right) + S_h \quad (10)$$

$$E = h - \frac{p}{\rho} + \frac{v^2}{2} \quad (11)$$

$$h = \sum_j Y_j h_j \quad (12)$$

where E is the internal energy, K_{eff} is the effective conductivity, h is the enthalpy and Y_i is the mass fraction. S_h is any external energy source that is unaccounted for.

The conservation of species of the flow is also written according to eq. 13 as:

$$\frac{\partial(\rho Y_i)}{\partial t} + \nabla\cdot(\rho\vec{v}Y_i) = -\nabla\cdot\vec{J}_i + R_i + S_i \quad (13)$$

where S_i is the sources term other than reaction and R_i is the addition or the destruction of the species due to the reaction and is expressed as:

$$R_{j,r} = R_{kin,r}\left(p_n - \frac{R_{j,r}}{D_{0,r}}\right)^N \quad (14)$$

where $R_{kin,r}$ is the Arrhenius reaction rate written as:

$$R_{kin,r} = A_r {T_p}^{\beta r} e^{-(E_r/RT_p)} \quad (15)$$

D_o is the effective surface area which is function of the localized temperature and particle diameter and is written as:

$$D_{0,r} = C_{1,r}\frac{[(T_p + T_\infty)/2]^{0.75}}{d_p} \quad (16)$$

The discrete Phase Model Equations that governs the Largrangian solid particles are expressed as:

$$\frac{du_p}{dt} = F_D\left(u - u_p\right) + \frac{g_x(\rho_p - \rho)}{\rho_p} + F_x \quad (17)$$

$$F_D = \frac{18\mu}{\rho_p {d_p}^2}\frac{C_D Re}{24} \quad (18)$$

$$Re = \frac{\rho d_p|u_p - u|}{\mu} \quad (19)$$

where F_D (u - u_p) is the drag force per unit particle mass; u is the fluid phase velocity; u_p is the particle velocity; and ρ is the fluid density, and ρ_p is the density of the particle. Equation (17) incorporates additional forces (F) in the particle force balance that can be important (i.e., thermophoretic and Brownian forces).

3.2. Model Setup and Boundary Conditions

The geometry and baseline mesh of the laboratory scale gasifier is depicted in Fig. 1 and detailed dimension and boundary conditions are summarized in Tables 3-4. This geometry matches the DTR which developed by the author group. It consisted of temperature controlled cylindrical tube of 154 cm length x 6.6 cm diameter and equipped with accurate dosing system. The DTR can be utilized to simulate the desired gasification environment.

Table 3: Boundary Condition for Validation

Boundary Condition	Value (Coal)
Length of Gasifier	1540 mm
Outer Diameter of Gasifier	75 mm
Inner Diameter of Gasifier	66 mm
Mass Flow Inlet	1.3320 g/s
Outer Wall Temperature	1,100C

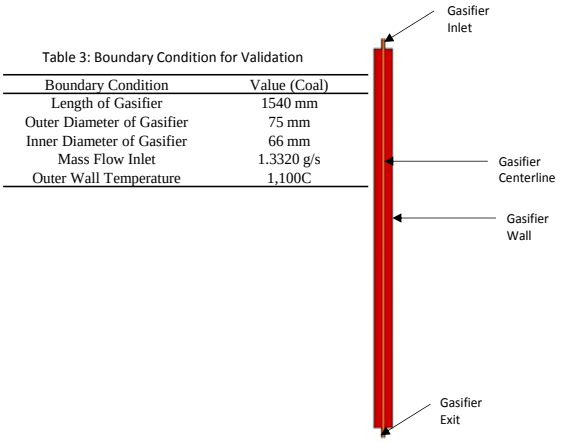

Fig. 1: Geometry and baseline mesh setup

Table 4: Boundary Condition for the Reactive Flow

Condition	Mix Pet 10%	Mix Pet 25%	Mix Pet 50%
O2 Inlet (g/s)	0.316	0.324	0.337
Particle Feed Rate (g/s)	0.234		
Wall Temp. (K)	1073-1273		
Equivalence Ratio	1.8		

3.3. Numerical Solution Approach

The numerical model of the gasification processes in an entrained flow gasifier was carried out within Ansys Fluent environment. As depicted in Fig. 2, the model uses Eulerian approach to solve the conservation of mass, species, momentum and energy for the continuous gas phase while uses the Lagrangian approach to discrete the feedstock particles to obtain their position, velocity and temperature. The particle-source-in cell approach was then used to couple the Eulerian and the Lagrangian approaches. Coupling of momentum, heat, and mass transfer between the solid and gas phases is accounted for by the two-way coupling Cloud model, in which Lagrangian-based particle trajectory is tracked as a cloud of particles about a mean trajectory. The mean trajectory is then calculated by solving the ensemble-averaged equations of motion for all particles represented by the cloud. The i^{th} species production/destruction due to the reaction r follows the eddy dissipation concept model used in other combustion/reaction flow work [14]. It uses the limited rate of either the instantaneous eddy-dissipation model that assumes the chemical reaction proceeds as the reactants meets and is faster than the time scale of the turbulence eddies or the Finite Arrhenius Rate model. The remaining solid char particle goes into the three gasification reactions as was detailed in Table 4.

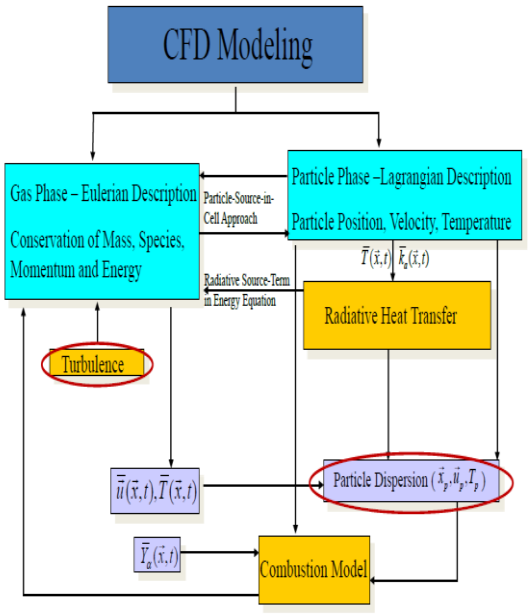

.

Fig. 2: Numerical solution approach for gasification [10]

4. Results and Discussions

4.1. Model Validation

The validity of the results of the model are tested against the experimental data of the drop tube reactor (DTR) at Masdar Institute Facilities. This DTR is instrumented with a calibrated dosing system, wall heat flux, and spatially distributed centerline and wall positioned thermocouples. It simulates the actual environment of the gasification within 120-150cm free entraining feedstock particles. The more the model results agree with the experimental values, the further fidelity in the model. Fig. 3 depicts the model results of the centerline temperature distribution and those measured experimentally for reactive flow using only coal as feedstock. The model results predict the experimental values reasonably well as seen in Fig. 3 [14].

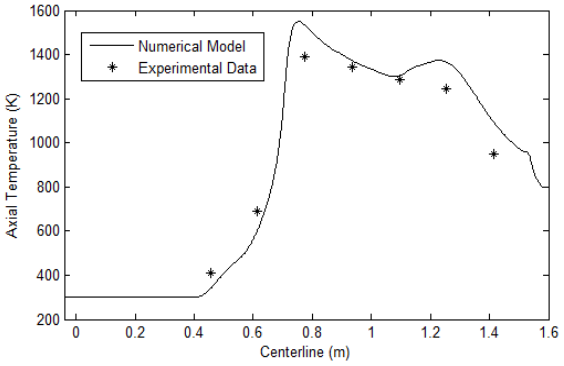

Fig. 3: Axial Temperature Validation with Experimental Data for Reactive Flow

4.2. Coal and Petcoke Co-Gasification

As indicated, co-firing petcock with coal offers dual advantages, refinery waste management and economical gain. The entrained flow gasifier accommodates fuel flexibility by allowing wider feedstock usage. For instance, an IGCC plant can utilize a combination of high coal quality and lower quality feedstock, like lignite, biomass, and even treated municipal solid waste for power generation. Fig. 4 depicts the temperature contour and the mole fraction of the volatile as well as the O_2 in the gasifier. The high temperature is delayed until the release of the moisture and volatile release, because these reactions are endothermic and despite the oxygen presence the partial combustion is insufficient to maximize the temperature neat the top entry zone. As soon as a higher temperature attained that triggered by the partial combustion, more volatile is released that simultaneously consumes the available O_2. This zone is coinciding with the highest DTR temperature which is somewhat located downstream the entry. The release of the volatile coincides with the exothermic volatile combustion which leads to the increase in the temperature around this region. The O_2 fraction is quickly reduced along the gasifier and reaches zero mole fraction also slightly downstream the top entry region. The reduction and the potential gas shift starts downstream along the reactor to normalize the production of syngas until the exit.

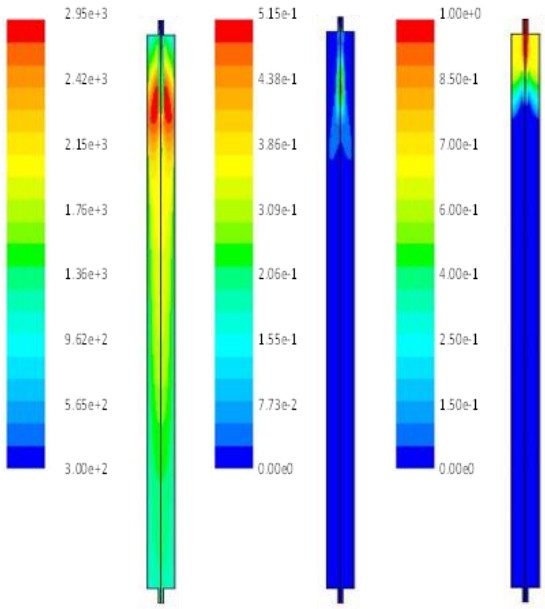

Fig. 4: (a) Temperature Contour (K), Left (b) Mole Fraction of Volatile, Middle (c) Mole Fraction of O_2, Right

Fig. 5 shows the contour of the mole fraction of the CO_2 and CO along the DTR/gasifier. Due to the volatile combustion, the CO_2 mole fraction was observed to increase along the gasifier and then decreased due to its reduction in the char-CO_2 equation according to equation 4. Consequently, this leads to the production of more CO downstream the DTR at the cost of reduction in temperature as was observed in the temperature distribution Fig. 4.

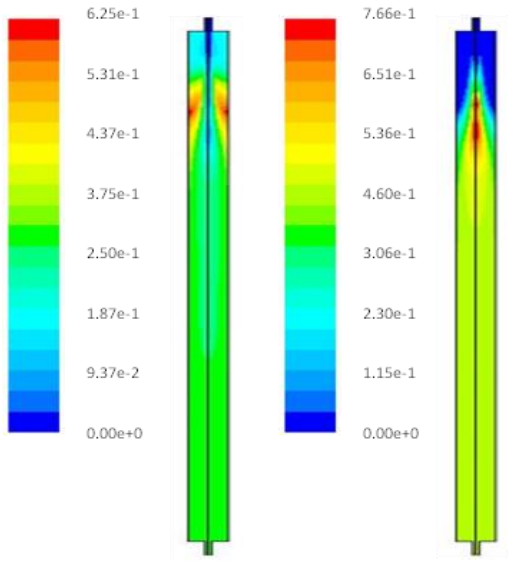

Fig. 5: (a) Mole Fraction of CO2, Left (b) Mole Fraction of CO, Right

Fig. 6 shows the contour of the mole fraction of the H_2O and H_2 along the gasifier. Due to the volatile combustion, the H_2O mole fraction was observed to increase along the gasifier and then decreased. The first increase due to combustion and its H_2O yield, while the decrease is attributed to the char-H_2O reaction per equation 5. Consequently, this leads to the production of more H_2 as flow goes down the drop tube and at the cost of reduction in the temperature as shown in Fig. 4.

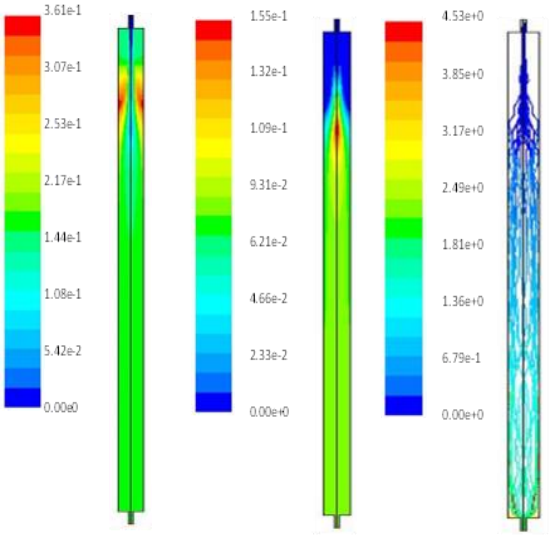

Fig. 6: (a) Mole Fraction of H_2O, Left (b) Mole Fraction of H_2, Middle (c) Particle Residence time (s)

4.3. Effect of Petroleum Coke Composition on Gasification

The effect of petroleum coke composition in the mixture of petroleum and Kentucky coal was studied in order to determine the optimum amount of petroleum coke to be used. It was observed that the syngas ($CO+H_2$) molar fraction is increased as the amount of petroleum coke in the mixture is increased. This is reasonable because at 50% mixture the amount of fixed carbon is the highest. Larger fixed carbon fraction implies more char reduction and as long as the temperature remains relatively high to do so more syngas production is expected. These results are presented in Fig. 7 and it follows the reactions described in equations 3-5.

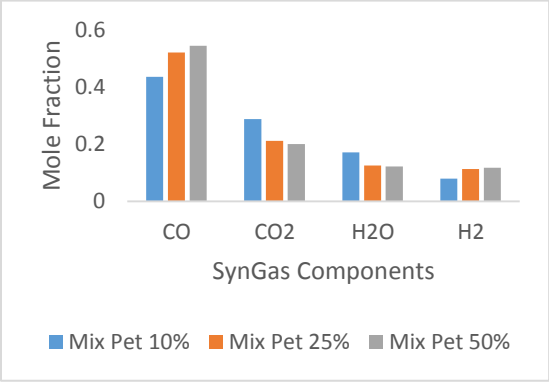

Fig. 7: Mole Fraction of SynGas for the three Mixing Ratios

The exit DTR temperature is accordingly decreased as one injects more petcoke in the mixture. The decrease in exit temperature is due to the high endothermic reaction of the fixed carbon reduction. The exit DTR temperature under different Petcoke/Coal mixing ratio is depicted in Fig. 8.

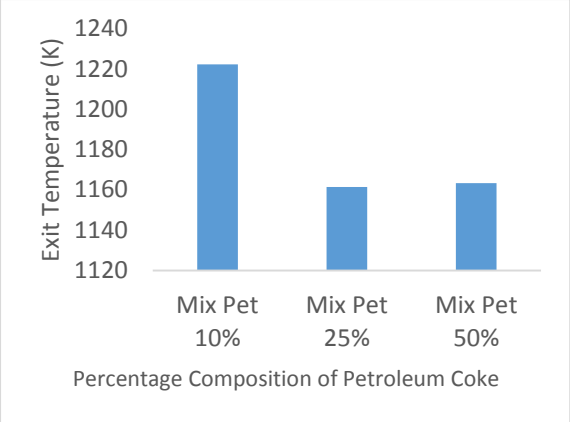

Fig. 8: Exit Temperature for the three Mixing Ratios

The residence time is also evaluated as longer residence time is inversely proportional to the gasifier throughput/capacity and also is a cost metric one needs to consider. In general one desires to use shorter gasifier which attains complete conversion and appropriate syngas production. Longer residence time is obtained at 50% mixture. One reason is the low density of the petroleum coke which was decreased when 50% petroleum coke is utilized as depicted in Fig. 9.

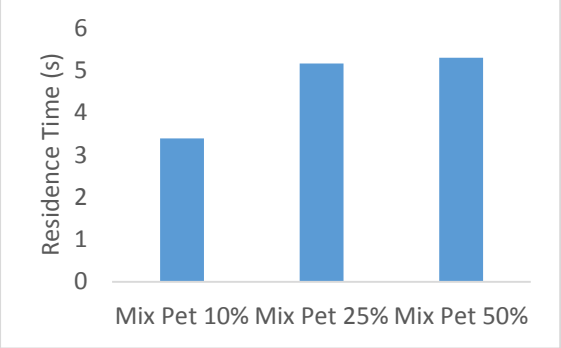

Fig. 9: Residence time for the three Mixing Ratios

4.4. Effect of Particle Size on Gasification

The effect of particle size (134nm, 334nm and 534nm) on the gasification mixture of 25% petroleum coke and -75% Kentucky coal was studied. It was generally observed that as the particle size increases, the yield of syngas (CO and H_2) decreases as depicted in Fig. 10. This is reasonable because smaller particle sizes give high surface area for reaction, thereby faster and more complete reaction as compared to larger particles. However, a new phenomenon was observed between 134 and 334 nm particle size. The syngas composition actually increases as the particle size increased from 134 nm to 334 nm. This may be attributed to other phenomena, such as quick volatile release and the combustion of smaller particle. The general trend, however, was confirmed at larger particle size of 543nm. The particle size of 334 nm gave the optimum syngas production.

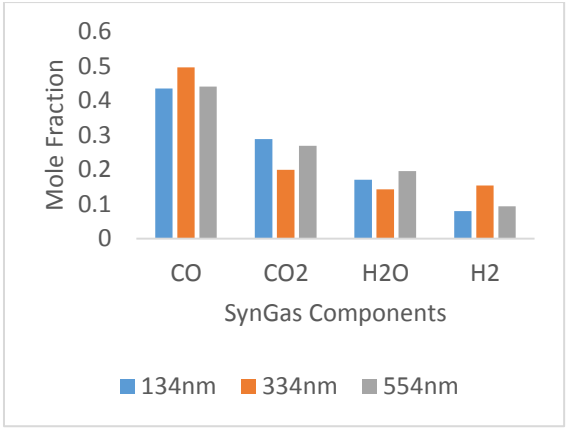

Fig. 10: Mole Fraction of SynGas for the three Particle Sizes

The temperature at the exit of the gasifier was observed to be the also lowest for 334 nm. This is favorable for gasification because the syngas has to be cooled down typically for post cleaning where a lower the exit temperature, the better the process metrics it becomes (Fig. 11).

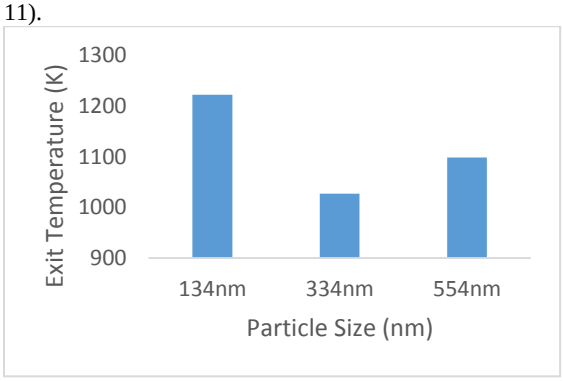

Fig. 11: Exit Temperature of SynGas for the three Particle Sizes

4.5. Effect of Wall Temperature on Gasification

The effect of wall temperature shows that the mole fraction of the syngas ($CO+H_2$) increases as the wall temperature is increased. The increase in wall temperature leads to a faster and better endothermic char gasification. The mole fraction of the syngas increased more sharply when the wall temperature is increased from 1,073 K to 1,173 K, but more gradual from 1,173 K to 1,273 K wall temperature. This shows that a temperature of 1,173 is the most suitable for the mixture of petroleum coke and Kentucky coal as presented in Fig. 12.

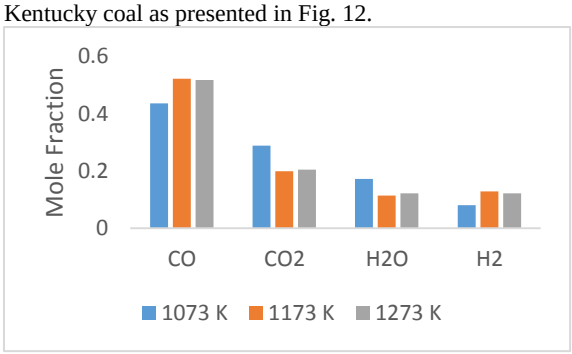

Fig. 12: Mole Fraction of SynGas for the three Wall Temperatures

5. Conclusions and Future Work

A comprehensive, predictive kinetics-based CFD model for the co-gasification of coal and petcoke has been investigated. The oxygen-blown atmospheric drop tube facility at Masdar Institute was used for as baseline for this setup. It was shown that the increases of Petcoke percentage leads to the production of more SynGas ($CO+H_2$). Decreasing the Particle size does not necessarily lead to the production of more SynGas ($CO+H_2$). Particle size of 334nm led to the highest SynGas production and lowest exit temperature. Wall temperature of 1,173 K led to the production of the most SynGas. The trend can be verified by examining more feedstock to observe the flexibility of the gasification system and specific adjustment for a particular fuel. Another research path the present work may take is the development of a detailed chemical mechanism for the gasification of feedstock and obtaining more data for the volatile composition during pyrolysis.

Acknowledgments

The support from Masdar Institute, the Waste to Energy group, and the MEG603-2015 class is highly acknowledged. Thanks also are due to Jennah Alonso for helping in preparation of the manuscript.

References

[1] Hampp F., "Development of experimental and numerical tools to investigate the thermochemical conversion of solid feedstock", Master's Thesis Dissertation, (2011) Masdar Institute.

[2] Chen, C., Horio, M., & Kojima, T., "Numerical simulation of entrained flow coal gasifiers. Part I: modeling of coal gasification in an entrained flow gasifier. Chemical Engineering Science", Vol.55 (2000) No. 18, 3861-3874.

[3] Watanabe, H., & Otaka, M., "Numerical simulation of coal gasification in entrained flow coal gasifier", Fuel, Vol. 85 (2006) No. 12, 1935-1943.

[4] Abani, N., & Ghoniem, A. F., "Large eddy simulations of coal gasification in an entrained flow gasifier", Fuel. Vol. 104 (2013) No. 31, 664-680.

[5] Ghenai, C., Janajreh, I., "CFD analysis of the effects of co-firing biomass with coal", Energy Conversion and Management, Vol. 51 (2010) No.8, 1694-1701.

[6] I. Adeyemi, I. Janajreh, T. Arink, C. Ghenai, "Gasification behavior of coal and woody biomass: Validation and parametrical study", Applied Energy 185 (2017) 1007–1018

[7] I. Janajreh, S. S. Raza, S. Elagroudy, "Co-Firing of Enteromorpha Prolifera Algae and RTC Coal in a Down Draft Gasifier: Material Characterization and Flow Simulation", J. Solid Waste Technology annd Management, Vo. 41, No. 1 (2015) 68-87.

[8] U.S. Environmental Protection Agency, Screening-Level Hazard Characterization, Petroleum Coke Category, June 2011; and H.W. Nelson, Petroleum Coke Handling Problems, 1970.

[9] H. Chris, and M. van der Burgt, "Gasification", Amsterdam, Boston: Gulf Professional Pub., 2003. ISBN: 0750677074

[10] Y. Yun, Y. Don Yoo, and S. Woo Chung, "Selection of IGCC candidate coals by pilot-scale gasifier operation", Fuel Processing Technology, Vol. 88, (2007), 107-116

[11] M. J. Prins, K. J. Ptasinski, and F. J.J. G. Janssen, "From coal to biomass gasification: Comparison of thermodynamic efficiency", Energy, Vol. 32, (2007), 1248-1259.

[12] Dhanaplan S, Annamalai K, Daripa P. Turbulent combustion modeling coal: biosolids blends in a swirl burner. Energy week, vol. IV. ETCE, ASME; (1997), 415–23.

[13] Ajay V. Kolhe, Rajesh E. Shelke, S. S. Khandare, "Combustion Modeling with CFD in Direct Injection CI Engine Fuelled with Biodiesel" , JJMIE, Vol. 9 (2015) No. 1, 61- 66